THE JOURNAL OF PHYSICAL CHEMISTRY Letters

pubs.acs.org/JPCL Letter

Neural Network Force Fields for Metal Growth Based on Energy Decompositions

Qin Hu, Mouyi Weng, Xin Chen, Shucheng Li, Feng Pan,* and Lin-Wang Wang*

Cite This: J. Phys. Chem. Lett. 2020, 11, 1364−1369 Read Online

ACCESS | Metrics & More | Article Recommendations | Supporting Information

ABSTRACT: A method using machine learning (ML) is proposed to describe metal growth for simulations, which retains the accuracy of ab initio density functional theory (DFT) and results in a thousands-fold reduction in the computational time. This method is based on atomic energy decomposition from DFT calculations. Compared with other ML methods, our energy decomposition approach can yield much more information with the same DFT calculations. This approach is employed for the amorphous sodium system, where only 1000 DFT molecular dynamics images are enough for training an accurate model. The DFT and neural network potential (NNP) are compared for the dynamics to show that similar structural properties are generated. Finally, metal growth experiments from liquid to solid in a small and larger system are carried out to demonstrate the ability of using NNP to simulate the real growth process.

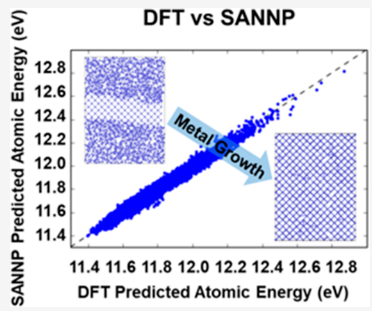

Machine learning and neural networks have been rapidly applied to many fields, including physics, medicine, biology, and chemistry.[1−5] It is now also widely attempted in materials science simulations.[6−9] Nevertheless, the field is still in its relative infancy, with many tests to be done and many areas to be explored. One major area is crystal growth. While a machine learning force field has been tested to predict ground-state properties extensively, there is a relative scarcity of reports using it to study nonequilibirum systems and phenomena like crystal growth. At the current stage, the metal crystal growth simulations can be divided into two major categories: one based on ab initio density functional theory (DFT), and the other based on semiempirical interatomic potentials or force fields (FFs), such as Stillinger−Weber potentials (SW) and the embedded atom method (EAM).[10−13] The choice of these methods depends on the consideration of accuracy and computational cost. Although high accuracy is the advantage of DFT calculation, it is often limited to the size of a few hundred atoms because of its high cost and $O(N^3)$ scaling. On the other hand, although it is relatively easy to simulate a system with thousands of atoms using FFs, its accuracy is not guaranteed. Very often, the empirical FFs are fitted to the macroscopic properties, e.g., the solid−liquid transition temperature, but the atomic level microscopic forces might not be correct, which can lead to an erroneous microscopic growth mechanism when compared to reality.

The machine learning force field has a potential to bridge the size gap between DFT simulation and the need for realistic growth simulation. It can retain the accuracy of DFT calculations at its atomic level, while still being capable of simulating systems with thousands of atoms. This is an intensely studied field. Currently, there are different approaches and different ML force fields, including generalized symmetry functions potential,[14] smooth overlapping of atomic potentials (SOAP),[15] bag of bonds (BoB) potential,[16] Gaussian approximation potentials (GAP),[17] deep tensor neural networks (DTNNs),[18] AGNI force field,[10] and deep potential molecular dynamics (DeePMD),[19] just to mention a few. Among these methods, Behler developed the original high-dimensional neural network potential (HDNNP) model which is most extensively used today.[20] All these potentials first map the local atomic structures into a set of features, which are rotational and permutational invariants. This set of features is then used as the input to fit the ab initio energy of the center atom. It is always assumed that the total energy of the whole system is a sum of the atomic energy, although the to-be-fitted atomic energy is actually unknown from an ab initio calculation. This significantly increases the uncertainty and also makes the training process nontrivial. It has been argued that using the total energy and the atomic forces alone might lead to an erroneous force field.[21] Thus, energy decomposition is a better method. For instance, Nakai proposed a method using the Hirshfeld partition for atomic partitioning.[22]

In this work, we applied our recently developed single-atom neural-network potential (SANNP) to the crystal growth of liquid Na. In the SANNP, during our DFT calculation, a procedure is used to decompose the total energy of the system into the atomic energy of each atom. We have shown that such atomic energy depends only on the local atomic environment; thus, it is amenable to ML training. However, SANNP has not

Received: December 19, 2019
Accepted: January 30, 2020
Published: January 30, 2020

https://dx.doi.org/10.1021/acs.jpclett.9b03780
J. Phys. Chem. Lett. 2020, 11, 1364−1369

been tested for crystal growth, which involves nonequilibrium properties like the diffusion rate and barrier heights. It is thus interesting to test such applications for SANNP. In addition, because of the availability of our atomic energy, we also take this opportunity to see how many DFT calculations are needed to fit a good SANNP in our approach. After all, one promise of ML-FF is to have a much faster turn-around time for force field development. Therefore, being able to train the force field quickly is essential.

Na metal is a relatively simple system. Such simple systems can usually be described well with the embedded atom method (EAM) force field. This allows us to compare our SANNP results with EAM results for large systems. Recently there has been renewed interest in Na metal. One application is for a Na battery because of the abundance of Na element (compared to lithium). The biggest challenge for a Na battery is its anode. Because there is no intercalation material for Na (unlike the graphene−Li anode), one possibility is to use Na metal. However, the Na metal has a serious platting issue, much worse than the Li metal anode. Thus, understanding the microscopic mechanism of Na crystal growth is critical. The liquid-to-solid growth is the simplest form of such Na crystal growth; thus, it is chosen as our testing ground for SANNP. We first carry out DFT molecular dynamics (MD) simulations for liquid and solid amorphous Na for the hundred-atom systems. This is then used to fit the SANNP. The fitted SANNP is then used to simulate liquid-to-solid crystal growth for large systems, and the results are then compared with EAM results.

The SANNP is a two hidden layers neural network model developed by Huang et al.,[23] which has been tested for Si. In this work, we focus on the metal element system Na. Much like HDNNP,[20] and most other models, in SANNP the total energy of a given system is assumed to be the simple sum of each atomic energy, $E_{tot} = \Sigma_i E_i$. The difference from other models is that, in the DFT calculation, we have developed a procedure to decompose the total energy E_{tot} into the atomic energy E_i. Thus, in this approach, the E_i is known. As a result, the energy data set is expanded by N times under the same DFT calculation, where N is the number of atoms in the DFT-calculated supercell, ranging from 100 to 300. Because the energy of the center atom depends on its neighbors for about 60 atoms, it will be problematic to use systems with less than 60 atoms (that will prevent the exploration of different local configurations). We thus use DFT systems that are a little bit larger than 60 atoms (e.g., around 100−300 atoms). The extra number of atoms will provide the buffer to reduce any correlation for the center 60 atoms. The force is also used in training, but only after the energy E_i is first trained; thus, a converged NN is already in shape. This is useful because the force training is much more complicated, more expensive, and more difficult to converge. In SANNP, a new set of features is also deployed. This set involves the pair feature, as well as three atom triangle features. As a result, the total number of features is around 300−400, which is larger than the numbers in other typical force fields (which is often on the order of 50−100). This increased number of features also requires more training data, which is provided by the decomposed atomic energy.

In the traditional classical force field, physical intuition is used to construct the energy terms, with parameters fitted to experiments or ab initio data. In ML, a much larger number of parameters are employed to flexibly fit any function, as used for the neural network. The meaning of these parameters is often difficult to explain; one can even think about the ML model as a high-dimensional interpolation scheme.[24] Thus, big data is an intrinsic component of such an approach. We first use the PWmat[25] to carry out ab initio MD and to get the decomposed atomic energy for every MD step. For the energy decomposition, the DFT calculation accuracy is similar to usual DFT MD calculations. For example, we typically require the self-consistent field (SCF) charge density relative error to be 1.0×10^{-3}, which is the same as for usual MD simulations. Sometimes, to play it safe, we have set the criterion to be 1.0×10^{-4}. However, that only increases the typical SCF steps per MD step from 2−3 steps to 4 steps. These data are then used in the training of NN weight and bias, using the back-propagation scheme for lost function derivatives, as implemented in the TensorFlow package. The whole training flowchart is shown in Scheme 1.

Scheme 1. Steps in Construction of Machine Learning Potentials

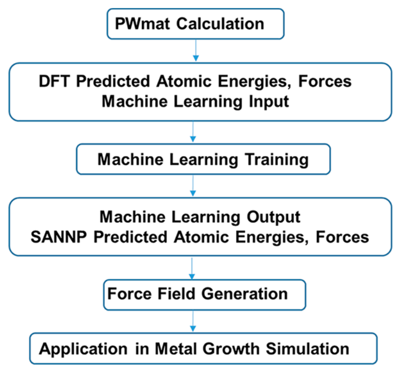

Our initial DFT-calculated system is a periodic box with 256 sodium atoms. The atoms run in four different temperatures (300, 500, 700, and 900 K) each for 1000 steps, and then the training data is taken in one snapshot for every four MD steps. This is equal to taking 250 steps from every temperature, so we have a set of 1000 DFT configurations. In this 1000 DFT data, 800 sets of data are used as the training set, while 100 points are used as a validation set, and 100 points are used as the testing set. In order to provide an uncorrelated testing and validation set, the last 200 snapshots are used as validation and testing set. The above four different temperatures cover the range of sodium melting, from solid to liquid. Figure S1 shows the total energy (E_{tot}), the sum of atomic energies ($\Sigma_i E_i$), and their differences at different temperatures.

In the training set, the results of the 800 DFT configurations correspond to 204 800 atomic energies and 614 400 atomic forces. According to the above training procedure, we get the test data with 100 configurations. The comparisons in atomic energies and forces are shown in Figure 1a,b. Indeed, because x, y, and z directions are kind of equivalent, we have removed the y and z directions for force in Figure S2. The potential calculated by the SANNP is close to the DFT results. The root mean squared error (RMSE) in E_i and F_i is approximately around 20 meV and 0.04 eV/Å in the test set; detailed data can be found in Table S1. Although we do not directly train against E_{tot}, E_{tot}^2 is related to E_i^2 by $\Delta E_{tot}^2 = \Sigma \Delta E_i^2$ (assuming no correlation between atoms, the explanation is shown in Figure S3.). The RMSE of the total energy per atom is thus

https://dx.doi.org/10.1021/acs.jpclett.9b03780
J. Phys. Chem. Lett. 2020, 11, 1364−1369

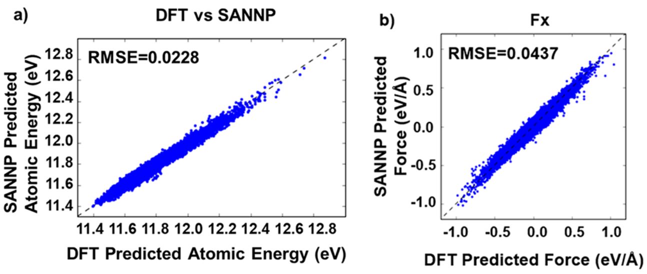

Figure 1. Comparison between DFT and SANNP for the test set with 100 configurations. (a) Comparison of DFT and SANNP atomic energies in the test set. (b) Comparison of DFT and SANNP forces in the test set.

$$\frac{\sqrt{\langle \Delta E_{\mathrm{tot}}^2 \rangle}}{N} = \frac{\sqrt{N \langle \Delta E_i^2 \rangle}}{N} \sim \frac{\sqrt{\langle \Delta E_i^2 \rangle}}{\sqrt{N}}$$

Thus, the RMSE of the total energy per atom is a factor of $1/\sqrt{(N)}$ smaller than the average RMSE of each individual atom. In our metal system, $N = 256$ ($1/\sqrt{(N)}$ approximately around 0.0625), so the RMSE of the total energy is around 1–3 meV/atom. This is consistent with many other reported errors in the literature.[23] This shows that, with our procedure, we can get a highly accurate force field with a relatively small number of DFT configurations. Note that, in previous literature,[20] especially to fit the neural-network model, sometimes tens of thousands of configurations are used. Our test demonstrates that decomposed atomic energy can be very helpful in terms of force field training.

Although the SANNP model is close to the DFT results, it is still necessary to compare DFT and SANNP for molecular dynamics simulation to guarantee that similar dynamic behaviors are reproduced. We choose *NVE* simulations to run the same system (256 sodium atoms) with SANNP at a temperature of 800 K. It is demonstrated that the energy is conserved, and the temperature fluctuates around 800 K in Figure 2a. Mean square displacement (MSD) and pair distribution function (PDF) are good quantities to represent the atomic diffusion and atomic structure of the system. MSD is directly related to the diffusion constant; we have used the Einstein equation to get the diffusion constant 0.00133 Å^2/fs. In Figure 2b,c, these curves of DFT and SANNP agree well, which demonstrates that the SANNP can be used to replace DFT to describe the dynamic behavior of the Na system.

We next apply the SANNP model to simulate the crystal growth from melt liquid. We first use the same periodic box with 256 sodium atoms in order to compare with DFT results. We fix the middle part and let other atoms move in 600 K, this results in the initial model of Figure 3a. Then, we separately use SANNP and DFT to simulate metal growth. The results are shown in panels b and c of Figure 3 for SANNP and DFT, respectively. Both SANNP and DFT grow into full crystal structure around 3200 fs, showing similar behavior and similar growth rate. SANNP has the advantage of speed. The calculations use the NVIDIA Titan X GPU as a computer resource. SANNP uses 1 GPU, and it takes 0.066 s per MD step for the SANNP calculation for 256 atoms. Running 8000 steps to get the crystal structure takes only about 9 min. DFT uses 4 GPUs, and for the same calculation using DFT, it takes about 27 h. The difference will become even greater for larger systems as the SANNP scales linearly to the size of the system, while the conventional DFT algorithm scales as $O(N^3)$.

To compare with the SANNP and DFT results, we have also carried out the crystal growth simulation using the embedded atom model (EAM) as implemented in Lammps.[26] For metallic systems, EAM is widely believed to be the best classical potential.[27] It has been widely used for metallic study, including growth. We note that, under the same initial and

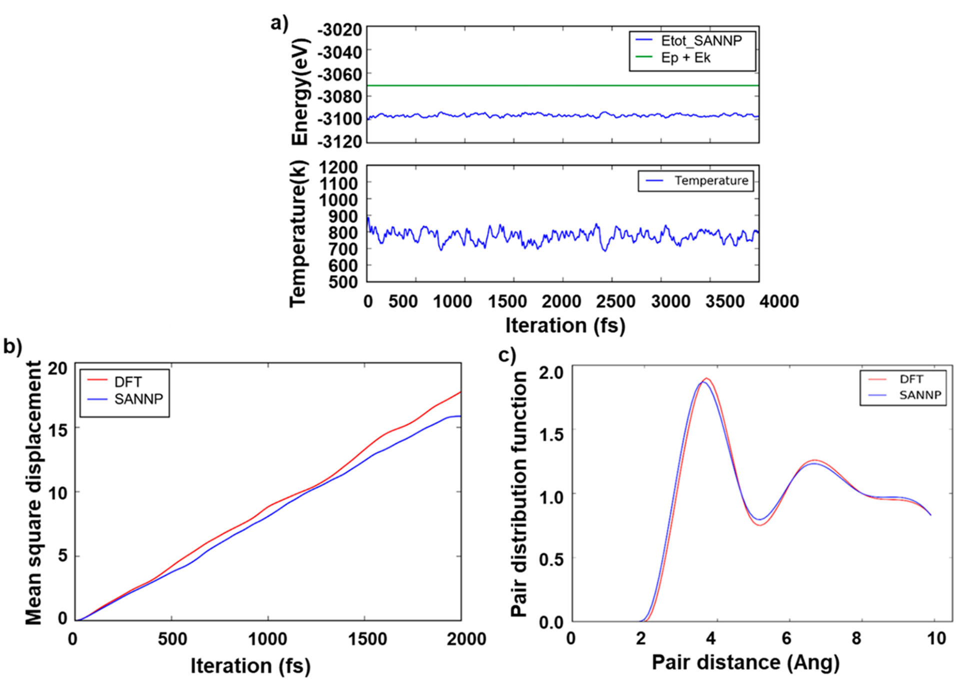

Figure 2. Dynamic behavior at 800 K. (a) Energy and temperature. Comparisons of mean square displacement (b) and pair distribution function (c) between DFT and SANNP.

https://dx.doi.org/10.1021/acs.jpclett.9b03780
J. Phys. Chem. Lett. 2020, 11, 1364−1369

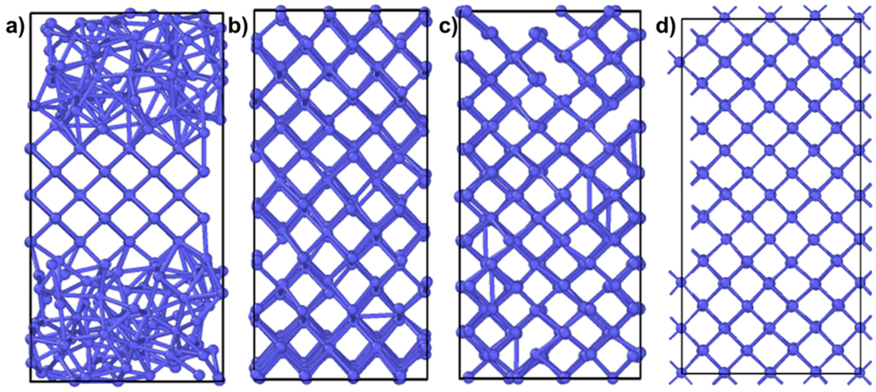

Figure 3. (a) Initial model of SANNP before simulation. Comparison among SANNP (b), DFT (c), and EAM (d) for metal growth simulation.

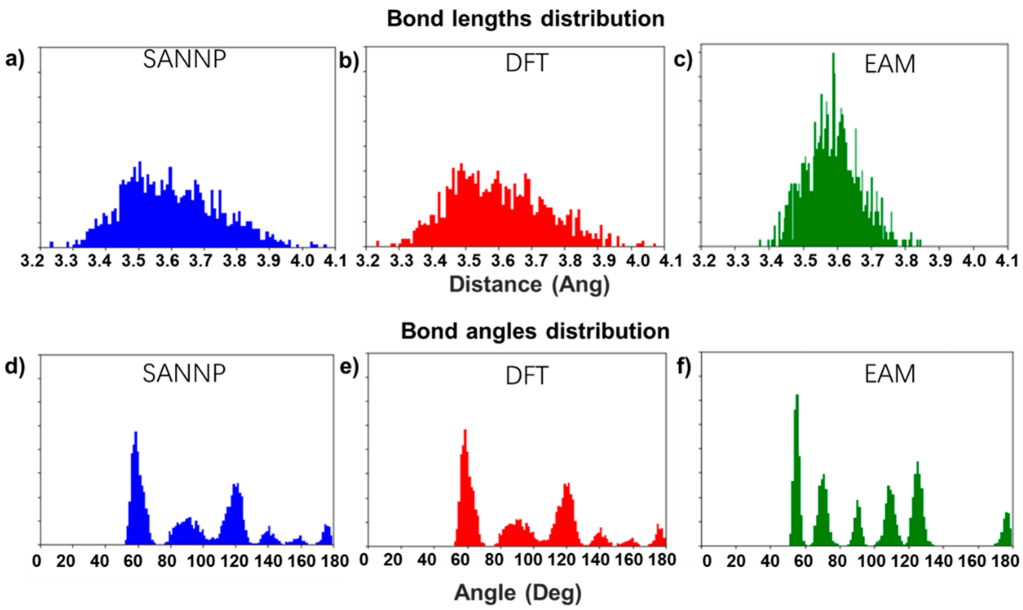

Figure 4. Comparison among SANNP (a and d), DFT (b and e), and EAM (c and f) for bond lengths and bond angle distribution.

temperature conditions, the time to reach the full crystal in the EAM simulation is around 1000 fs (compared to the 3200 fs used by both SANNP and DFT). Second, as shown in Figure 3d, the final structure is much more rigid than that of SANNP and DFT. To plot the bond, a 3.8 Å cutoff is used. As one can see, using such a cutoff for SANNP and DFT results, we can find additional bonds, as well as missing bonding from a perfect BCC structure. Thus, no matter what cutoff is used, there are always such imperfections (missing or additional bonds). To illustrate this difference more quantitatively, we have calculated the bond length and bond angle distributions for comparison. The results are shown in Figure 4a−c for bond lengths and Figure 4d−f for bond angles. In the EAM data, the distribution is narrower; this indicates that the crystal is more rigid. A more striking difference comes from the angle distribution. We see the pattern is different, showing a higher resolution for the angle due to smaller lattice fluctuations. In comparison with DFT and EAM simulations, the SANNP is much faster than DFT and much more accurate than EAM. Thus, using SANNP represents a new approach to studying the dynamic behavior of metallic systems.

For the larger system, we have built a new periodic system with 1536 sodium atoms. In the beginning, some atoms are in the crystal phase, while others are in a disordered liquid phase. This can thus be used to study the nucleation process. This structure for the initial model is shown in Figure 5a. The experimental Na solid−liquid transition temperature is at T_c = 370 K. We set the temperature to 50 K, corresponding to an overcooled liquid. We then run the molecular dynamics simulation for 8000 steps. It can be found that (Figure 5b) there is already significant crystal growth after 2000 fs. In some covalent bonding crystals (e.g., Si), the growth usually happens along a surface step (e.g., one additional layer extended from one side of the surface to another side). We note that the growth happens not along with any surface steps, but directly grows in the surface normal direction along with large fluctuation. This is in agreement with previous metal crystal growth simulation results. Figure 5c shows the final crystal with SANNP after completed growth around 4000 fs. The final crystal with EAM is also shown in Figure 5d. The EAM result is more regular, and it takes only 1200 fs to complete the growth, more than 3 times faster than the SANNP result. We thus found a significant difference between SANNP and EAM behavior. Given the similarity between the SANNP and DFT growth in smaller systems, it will thus be much more accurate to use SANNP to study the crystal growth (e.g., defect and dislocation formation) in the future.

https://dx.doi.org/10.1021/acs.jpclett.9b03780
J. Phys. Chem. Lett. 2020, 11, 1364−1369

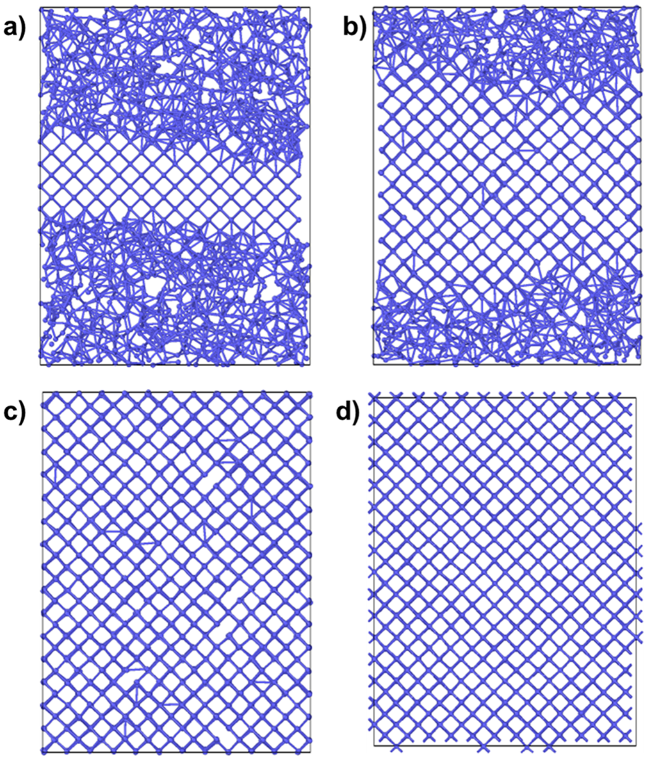

Figure 5. Metal growth simulation for a large system. (a) The initial model of SANNP. (b) Growing state with SANNP. (c) Final crystal with SANNP. (d) Final crystal with EAM.

In summary, we tested the SANNP method for a Na system, in particular, applying it to melt Na crystal growth. We found that the DFT calculation with energy decomposition can provide an efficient way of training SANNP. One thousand configurations are sufficient to provide enough data to fit the SANNP potential. The fitted SANNP compares well with the DFT result in both its atomic energy and force, as well as the dynamic behavior of the systems: the mean square displacement, the pair distribution function, and the crystal growth speed. On the other hand, the SANNP simulation is hundreds of times faster. We have also applied the SANNP to larger systems to simulate the crystal growth, and we compare that with EAM results. We found that there are significant differences between SANNP results and EAM results, in terms of crystal fluctuations as well as the crystal growth rate. Overall, we expect ML potentials like SANNP can serve as powerful tools to study the nonequilibirum dynamic behavior of metals in the future.

■ ASSOCIATED CONTENT

Supporting Information

The Supporting Information is available free of charge at https://pubs.acs.org/doi/10.1021/acs.jpclett.9b03780.

More technique details, including the energy of mix temperatures; comparison of DFT and SANNP forces Fy, Fz in the test set; RMSE and mean absolute error in E_i and F_i; the functional relationship between $\Delta E_{\mathrm{tot}}^2$ and $\Sigma\Delta E_i^2$; temperature variation with time for SANNP, DFT, and EAM; detail of energy decompositions; method of energy decompositions; structural data (PDF)

■ AUTHOR INFORMATION

Corresponding Authors

Feng Pan − *School of Advanced Materials, Peking University Shenzhen Graduate School, Shenzhen 518055, China;* orcid.org/0000-0002-8216-1339; Email: panfeng@pkusz.edu.cn

Lin-Wang Wang − *Materials Sciences Division, Lawrence Berkeley National Laboratory, Berkeley, California 94720, United States*; Email: lwwang@lbl.gov

Authors

Qin Hu − *School of Advanced Materials, Peking University Shenzhen Graduate School, Shenzhen 518055, China*

Mouyi Weng − *School of Advanced Materials, Peking University Shenzhen Graduate School, Shenzhen 518055, China*

Xin Chen − *School of Advanced Materials, Peking University Shenzhen Graduate School, Shenzhen 518055, China*

Shucheng Li − *School of Advanced Materials, Peking University Shenzhen Graduate School, Shenzhen 518055, China*

Complete contact information is available at: https://pubs.acs.org/10.1021/acs.jpclett.9b03780

Notes

The authors declare no competing financial interest.

■ ACKNOWLEDGMENTS

We thank Dr. Ling Miao for inspiring discussions. This work was supported by the Director, Office of Science (SC), Basic Energy Science (BES), Materials Science and Engineering Division (MSED), of the US Department of Energy (DOE) through the in situ TEM program (KC22ZH) under Contract No. DE-AC02-05CH11231. This work was also financially supported by the National Key R&D Program of China (2016YFB0700600), Soft Science Research Project of Guangdong Province (2017B030301013), and Shenzhen Science and Technology Research Grant (ZDSYS201707281026184).

■ REFERENCES

(1) Carleo, G.; Troyer, M. Solving the quantum many-body problem with artificial neural networks. *Science* **2017**, *355*, 602−605.

(2) Ciodaro, T.; Deva, D.; de Seixas, J. M.; Damazio, D. Online particle detection with Neural Networks based on topological calorimetry information. *J. Phys.: Conf. Ser.* **2012**, *368*, 012030.

(3) Helmstaedter, M.; Briggman, K. L.; Turaga, S. C.; Jain, V.; Seung, H. S.; Denk, W. Connectomic reconstruction of the inner plexiform layer in the mouse retina. *Nature* **2013**, *500*, 168−174.

(4) Krenn, M.; Malik, M.; Fickler, R.; Lapkiewicz, R.; Zeilinger, A. Automated Search for new Quantum Experiments. *Phys. Rev. Lett.* **2016**, *116*, 090405.

(5) Libbrecht, M. W.; Noble, W. S. Machine learning applications in genetics and genomics. *Nat. Rev. Genet.* **2015**, *16*, 321−332.

(6) Butler, K. T.; Davies, D. W.; Cartwright, H.; Isayev, O.; Walsh, A. Machine learning for molecular and materials science. *Nature* **2018**, *559*, 547−555.

(7) Zhang, L.; Han, J.; Wang, H.; Car, R.; E, W. Deep Potential Molecular Dynamics: A Scalable Model with the Accuracy of Quantum Mechanics. *Phys. Rev. Lett.* **2018**, *120*, 143001.

(8) Jie, J.; Weng, M.; Li, S.; Chen, D.; Li, S.; Xiao, W.; Zheng, J.; Pan, F.; Wang, L.-W. A new Material Go database and its comparison with other high-throughput electronic structure databases for their predicted energy band gaps. *Sci. China: Technol. Sci.* **2019**, *62*, 1423−1430.

(9) Jie, J.; Hu, Z.; Qian, G.; Weng, M.; Li, S.; Li, S.; Hu, M.; Chen, D.; Xiao, W.; Zheng, J.; et al. Discovering unusual structures from

exception using big data and machine learning techniques. *Science Bulletin* **2019**, *64*, 612−616.
(10) Botu, V.; Batra, R.; Chapman, J.; Ramprasad, R. Machine Learning Force Fields: Construction, Validation, and Outlook. *J. Phys. Chem. C* **2017**, *121*, 511−522.
(11) Burke, K. Perspective on density functional theory. *J. Chem. Phys.* **2012**, *136*, 150901.
(12) Hautier, G.; Jain, A.; Ong, S. P. From the computer to the laboratory: materials discovery and design using first-principles calculations. *J. Mater. Sci.* **2012**, *47*, 7317−7340.
(13) Hill, J. R.; Freeman, C. M.; Subramanian, L. Use of force fields in materials modeling. *Rev. Comput. Chem.* **2007**, *16*, 141−216.
(14) Behler, J. Atom-centered symmetry functions for constructing high-dimensional neural network potentials. *J. Chem. Phys.* **2011**, *134*, 074106.
(15) Bartók, A. P.; Kondor, R.; Csányi, G. On representing chemical environments. *Phys. Rev. B: Condens. Matter Mater. Phys.* **2013**, *87*, 184115.
(16) Hansen, K.; Biegler, F.; Ramakrishnan, R.; Pronobis, W.; von Lilienfeld, O. A.; Müller, K.-R.; Tkatchenko, A. Machine Learning Predictions of Molecular Properties: Accurate Many-Body Potentials and Nonlocality in Chemical Space. *J. Phys. Chem. Lett.* **2015**, *6*, 2326−2331.
(17) Deringer, V. L.; Csanyi, G. Machine learning based interatomic potential for amorphous carbon. *Phys. Rev. B: Condens. Matter Mater. Phys.* **2017**, *95*, 094203.
(18) Schütt, K. T.; Arbabzadah, F.; Chmiela, S.; Müller, K. R.; Tkatchenko, A. Quantum-chemical insights from deep tensor neural networks. *Nat. Commun.* **2017**, *8*, 13890.
(19) Zhang, L.; Han, J.; Wang, H.; Car, R.; E, W. Deep Potential Molecular Dynamics: A Scalable Model with the Accuracy of Quantum Mechanics. *Phys. Rev. Lett.* **2018**, *120*, 143001.
(20) Behler, J.; Parrinello, M. Generalized neural-network representation of high-dimensional potential-energy surfaces. *Phys. Rev. Lett.* **2007**, *98*, 146401.
(21) Kang, J.; Wang, L.-W. First-principles Green−Kubo method for thermal conductivity calculations. *Phys. Rev. B: Condens. Matter Mater. Phys.* **2017**, *96*, 020302.
(22) Nakai, H. Energy density analysis with Kohn-Sham orbitals. *Chem. Phys. Lett.* **2002**, *363*, 73−79.
(23) Huang, Y.; Kang, J.; Goddard, W. A., III; Wang, L.-W. Density functional theory based neural network force fields from energy decompositions. *Phys. Rev. B: Condens. Matter Mater. Phys.* **2019**, *99*, 064103.
(24) Rumelhart, D. E.; Hinton, G. E.; Williams, R. J. Learning representations by back-propagating errors. *Nature* **1986**, *323*, 533−536.
(25) Jia, W.; Fu, J.; Cao, Z.; Wang, L.; Chi, X.; Gao, W.; Wang, L.-W. Fast plane wave density functional theory molecular dynamics calculations on multi-GPU machines. *J. Comput. Phys.* **2013**, *251*, 102−115.
(26) Plimpton, S. Fast Parallel Algorithms for Short-Range Molecular Dynamics. *J. Comput. Phys.* **1995**, *117*, 1−19.
(27) Metya, A. K.; Hens, A.; Singh, J. K. Molecular dynamics study of vapor-liquid equilibria and transport properties of sodium and lithium based on EAM potentials. *Fluid Phase Equilib.* **2012**, *313*, 16−24.

https://dx.doi.org/10.1021/acs.jpclett.9b03780
J. Phys. Chem. Lett. 2020, 11, 1364−1369